Available online at www.sciencedirect.com
SCIENCE DIRECT®
Journal of Computational Physics 200 (2004) 34–49
JOURNAL OF COMPUTATIONAL PHYSICS
www.elsevier.com/locate/jcp

A spectral collocation method to solve Helmholtz problems with boundary conditions involving mixed tangential and normal derivatives

S. Nguyen, C. Delcarte *

Université Paris-Sud XI, LIMSI-CNRS, B.P. 133, 91403 Orsay Cedex, France

Received 27 June 2003; received in revised form 22 March 2004; accepted 22 March 2004
Available online 21 April 2004

Abstract

The performing spectral method, developed by Haldenwang et al. [J. Comput. Phys. 55 (1984) 115], to solve multi-dimensional Helmholtz equations, associated to mixed boundary conditions with constant coefficients, is extended to boundary conditions mixing a first order normal derivative with a second order tangential derivative. The accuracy of the proposed algorithm is evaluated on two test cases for which analytical solutions exist: an academic problem and a physical configuration including an interface with shear viscosity. The procedure is also applied to the research of the Rayleigh–Bénard instability thresholds in closed cavities with thin diffusive walls.

Keywords: Helmholtz equation; Collocation spectral method

1. Introduction

The Navier–Stokes and energy equations associated with boundary conditions mixing a normal derivative to a second order tangential derivative are encountered in many physical systems such as fluids confined within walls of arbitrary thermal conductivity [5] or in flows involving an interface with shear viscosity [10]. This type of condition arises whenever a boundary is subjected to a coupling between flux and intrinsic interfacial dissipation of some physical quantity.

Conservation equations are often transformed into Helmholtz problems which can be solved using a direct Chebyshev collocation method as developed by Dang-Vu and Delcarte [8]. This method leads to the resolution of quasi-tridiagonal systems. Though avoiding any iterative algorithm, and offering a very accurate solution, this procedure is slower than the one proposed by Haidvogel and Zang [4] in the case of time dependent problems for which a Helmholtz equation has to be solved at each time step. Haldenwang

* Corresponding author.
E-mail addresses: snguyen@limsi.fr (S. Nguyen), delcarte@limsi.fr (C. Delcarte).

0021-9991/$ - see front matter
doi:10.1016/j.jcp.2004.03.004

et al. [6] have proposed a performing 3D spectral solver for the Helmholtz equation in case of Dirichlet, Neumann or Robin (mixed) boundary conditions with constant coefficients. This method, based on successive diagonalisations of the second order derivatives of the Helmholtz operator, allows to reduce efficiently the computing time and is relevant to time dependent problems. In this paper, we propose an extension of this method to boundary conditions mixing a normal derivative to a second order tangential derivative.

The general formulation of the method is presented in Section 2, the corresponding algorithm is detailed in Section 3, and validated in Section 4 through comparisons with analytical solutions of mathematical and physical configurations. Results of the literature on the thermal stability of a fluid contained in a rectangular enclosure heated from below are reproduced and extended. The CPU cost of the proposed algorithm is estimated on this time dependent problem. Section 5 presents the conclusions.

2. Description of the problem and method of solution

We consider the 2D Helmholtz problem in Cartesian coordinates

$$\frac{\partial^2 u}{\partial x^2}+\frac{\partial^2 u}{\partial z^2}-au=f,\quad x,z,\in[-1,1],\ \ a>0, \tag{1}$$

where u and f are, respectively, the solution and a source term, x and z being the horizontal and vertical directions. The following boundary conditions are imposed:

$$u\in\partial\Omega\begin{cases}\alpha_{1\pm}\frac{\partial^2 u}{\partial z^2}+\beta_{1\pm}\frac{\partial u}{\partial x}=\gamma_{1\pm}(z) & \text{at } x=\pm1 \quad \text{(a)}\\ \alpha_{2\pm}u=\gamma_{2\pm}(x) & \text{at } z=\pm1 \quad \text{(b)}.\end{cases} \tag{2}$$

$\alpha_{1\pm}$, $\alpha_{2\pm}$ and $\beta_{1\pm}$ are constant (Fig. 1).

For clarity's sake, the method is developed in case of Dirichlet conditions along one set of parallel boundaries with $\gamma_{2\pm}$ depending on the position on the boundary. Its extension to Neumann or Robin conditions and to 3D configurations is then explained.

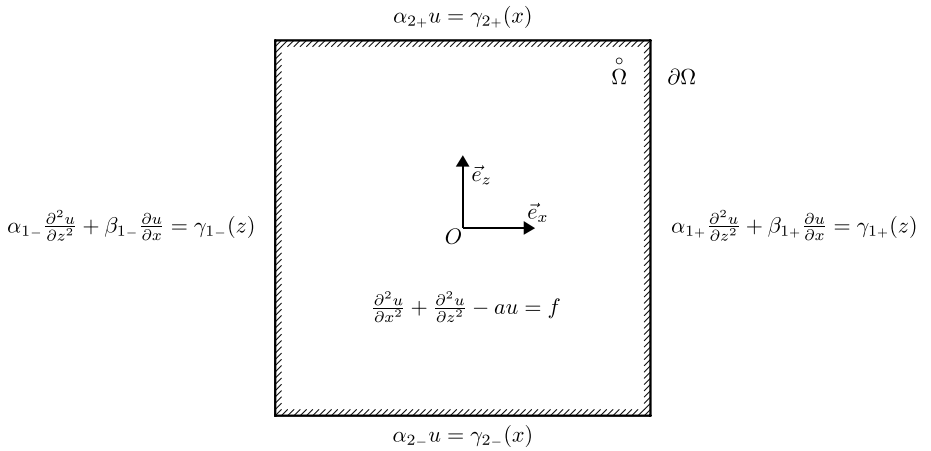

Fig. 1. 2D scalar Helmholtz problem with Dirichlet conditions at $z=\pm1$ and a second tangential derivative mixed with a Neumann condition at $x=\pm1$.

The extension by Haldewang et al. [6] of the diagonalisation technique proposed by Haidvogel and Zang [4] to the case of Robin conditions is based on the reduction of the system, resulting from a Chebyshev collocation approximation, by algebraic elimination of the boundary conditions. The algorithm then proceeds to successive diagonalisations in each direction of the system reduced to the inner domain, the eigenvalues of the total operator being the sum of the eigenvalues of three 1D operators.

If the coefficients in the Robin conditions are space dependent, the elimination process leads to a modified non-tensoriable Helmholtz operator. Nevertheless a solution may still be computed with spectral accuracy using an iterative algorithm as proposed by Delcarte et al. [11].

When a boundary condition involves normal as well as tangential derivatives, a reduction of the system as done in [6] or [11] does not allow successive diagonalisations because each boundary point is then coupled to each inner point, while in Haldenwang's case, one boundary point is at most coupled to the inner points along the normal direction to the boundary. Of course, a solution can then consist of constructing explicitly the total Helmholtz operator and calculating its inverse. Though it preserves the spectral accuracy, it is both costly in memory and computation time.

The basic idea of our method is to transform the mixed condition into a Robin condition in finding $\zeta\pm$ functions such that

$$\alpha_{1\pm}\left.\frac{\partial^2 u}{\partial z^2}\right|_{x=\pm 1} = \zeta_{\pm}(z)u|_{x=\pm 1}. \tag{3}$$

Eq. (3) is a well-known eigenvalue problem. This suggests rewriting the problem in the basis of the eigenvectors of $\partial^2/\partial z^2$. Nevertheless, it is necessary, first, to remove the zero eigenvalues of the second order derivative matrix by cancelling out the utmost points of the horizontal boundaries.

The algorithm proposed below is based on these considerations. As it will be shown, compared with Haldenwang et al. [6] procedure, it preserves the spectral accuracy with a reasonable memory cost increase and a computation time of the same order.

3. The algorithm

3.1. The discrete problem

We use a Chebyshev collocation spectral method on a Gauss–Lobatto grid [2,3]. The collocation points along $\vec{e}_x$ and $\vec{e}_z$ are given by

$$x_i = -\cos\left(\frac{i\pi}{N_x}\right), \quad i \in \{0,\ldots,N_x\}, \tag{4a}$$

$$z_j = -\cos\left(\frac{j\pi}{N_z}\right), \quad j \in \{0,\ldots,N_z\}. \tag{4b}$$

The discrete Helmholtz problem reads

$$\sum_{k=0}^{N_x}(\mathscr{D}_x^2)_{ik}u_{kj} + \sum_{l=0}^{N_z}(\mathscr{D}_z^2)_{jl}u_{il} - au_{ij} = f_{ij}, \quad i \in \{0,\ldots,N_x\} \text{ and } j \in \{0,\ldots,N_z\}, \tag{5}$$

associated with the set of boundary conditions:

$$u \in \partial\Omega\begin{cases} \alpha_{1\pm}\sum_{l=0}^{N_z}(\mathscr{D}_z^2)_{jl}u_{|_0^{N_x}l} + \beta_{1\pm}\sum_{k=0}^{N_x}(\mathscr{D}_x)_{|_0^{N_x}k}u_{kj} = \gamma_{1\pm}(j) & \text{for } j \in \{0,\ldots,N_z\} \quad \text{(a)} \\ \alpha_{2\pm}u_{i|_0^{N_z}} = \gamma_{2\pm}(i) & \text{for } i \in \{0,\ldots,N_x\} \quad \text{(b)} \end{cases} \tag{6}$$

with $\gamma_{1\pm}(j) = \gamma_{1\pm}(z_j)$ and $\gamma_{2\pm}(i) = \gamma_{2\pm}(x_i)$. $\mathscr{D}_z^x$ denotes the first derivative spectral operator with respect to $\binom{x}{z}$ and $\mathscr{D}_z^{2x}$ the second derivative operator $[\mathscr{D}_z^{2x}]_{ij} = \sum_k [\mathscr{D}_z^x]_{ik} \cdot [\mathscr{D}_z^x]_{kj}$.

3.2. The procedure

Step 1: Elimination of the Dirichlet boundary conditions.

In the configuration here considered, we eliminate the horizontal boundaries (6)b. The discrete Helmholtz equation becomes

$$\sum_{k=0}^{N_x} (\mathscr{D}_x^2)_{ik} u_{kj} + \sum_{l=1}^{N_z-1} (\mathscr{D}_z^2)_{jl} u_{il} - a u_{ij} = f'_{ij}, \quad i \in \{0,\dots,N_x\},\ j \in \{1,\dots,N_z-1\}$$

$$\text{with } f'_{ij} = f_{ij} - \{(\mathscr{D}_z^2)_{j0} u_{i0} + (\mathscr{D}_z^2)_{jN_z} u_{iN_z}\} \text{ and } u_{i|_0^{N_z}} = \frac{\gamma_{2\pm}(i)}{\alpha_{2\pm}}. \tag{7}$$

The remaining boundary conditions are written as

$$\alpha_{1\pm} \sum_{l=1}^{N_z-1} (\mathscr{D}_z^2)_{jl} u_{|_0^{N_x} l} + \beta_{1\pm} \sum_{k=0}^{N_x} (\mathscr{D}_x)_{|_0^{N_x} k} u_{kj} = \gamma_{1\pm}(j) - \{(\mathscr{D}_z^2)_{j0} u_{|_0^{N_x} 0} + (\mathscr{D}_z^2)_{jN_z} u_{|_0^{N_x} N_z}\}, \quad j \in \{1,\dots,N_z-1\}. \tag{8}$$

Step 2: Change of basis.

Let us define $(\mathscr{D}_z^2)_{\text{int}}$ as the inner part of $(\mathscr{D}_z^2)$: $[(\mathscr{D}_z^2)_{\text{int}}]_{jl} = (\mathscr{D}_z^2)_{jl}$ for $j,l \in \{1,\dots,N_z-1\}$. The reduced Helmholtz equation and the associated boundary conditions are now expressed in the basis of the eigenvectors of $(\mathscr{D}_z^2)_{\text{int}}$. $\mathscr{M}_z$ being the matrix of the eigenvectors of $(\mathscr{D}_z^2)_{\text{int}}$

$$\mathscr{M}_z^{-1} (\mathscr{D}_z^2)_{\text{int}} \mathscr{M}_z = \Lambda_z^2, \quad (\Lambda_z^2)_{jl} = \delta_{jl} (\lambda_z)_j, \quad j \in \{1,\dots,N_z-1\}.$$

We introduce the following notations for $i \in \{0,\dots,N_x\}$ and $j \in \{1,\dots,N_z-1\}$:

$$\tilde{u}_{ij} = \sum_{l=1}^{N_z-1} (\mathscr{M}_z^{-1})_{jl} u_{il}, \quad \tilde{f}'_{ij} = \sum_{l=1}^{N_z-1} (\mathscr{M}_z^{-1})_{jl} f'_{il},$$

$$\tilde{\alpha}_{1\pm}(j) = \alpha_{1\pm} . (\lambda_z)_j, \quad \tilde{\beta}_{1\pm} = \beta_{1\pm},$$

$$\tilde{\gamma}'_{1\pm}(j) = \sum_{l=1}^{N_z-1} (\mathscr{M}_z^{-1})_{jl} \Big[\gamma_{1\pm}(l) - \{(\mathscr{D}_z^2)_{l0} u_{|_0^{N_x} 0} + (\mathscr{D}_z^2)_{lN_z} u_{|_0^{N_x} N_z}\}\Big].$$

In this new basis, the discretised Helmholtz problem, for $i \in \{0,\dots,N_x\}$ and $j \in \{1,\dots,N_z-1\}$, reads

$$\sum_{k=0}^{N_x} (\mathscr{D}_x^2)_{ik} \tilde{u}_{kj} + \sum_{l=1}^{N_z-1} (\Lambda_z^2)_{jl} \tilde{u}_{il} - a \tilde{u}_{ij} = \tilde{f}'_{ij} \tag{9}$$

with the mixed boundary conditions

$$\tilde{\alpha}_{1\pm}(j) \tilde{u}_{|_0^{N_x} j} + \tilde{\beta}_{1\pm} \sum_{k=0}^{N_x} (\mathscr{D}_x)_{|_0^{N_x} k} \tilde{u}_{kj} = \tilde{\gamma}'_{1\pm}(j). \tag{10}$$

Step 3: Elimination of the mixed conditions.

To eliminate the boundary points $\tilde{u}_{0j}$ and $\tilde{u}_{N_x j}$, we express them in terms of the inner points thanks to the two mixed boundary conditions

$$(\tilde{\alpha}_{1-}(j) + \tilde{\beta}_{1-}(\mathscr{D}_x)_{00})\tilde{u}_{0j} + \tilde{\beta}_{1-}\sum_{k=1}^{N_x-1}(\mathscr{D}_x)_{0k}\tilde{u}_{kj} + \tilde{\beta}_{1-}(\mathscr{D}_x)_{0N_x}\tilde{u}_{N_xj} = \tilde{\gamma}'_{1-}(j), \tag{11}$$

$$(\tilde{\alpha}_{1+}(j) + \tilde{\beta}_{1+}(\mathscr{D}_x)_{N_xN_x})\tilde{u}_{N_xj} + \tilde{\beta}_{1+}\sum_{k=1}^{N_x-1}(\mathscr{D}_x)_{N_xk}\tilde{u}_{kj} + \tilde{\beta}_{1+}(\mathscr{D}_x)_{N_x0}\tilde{u}_{0j} = \tilde{\gamma}'_{1+}(j). \tag{12}$$

The resolution of the linear system $\begin{cases}(11)\\(12)\end{cases}$ leads to the following relations:

$$\tilde{u}_{0j} = \sum_{k=1}^{N_x-1}\tilde{v}^-_{jk}\tilde{u}_{kj} + \tilde{\mu}^-_j, \tag{13a}$$

$$\tilde{u}_{N_xj} = \sum_{k=1}^{N_x-1}\tilde{v}^+_{jk}\tilde{u}_{kj} + \tilde{\mu}^+_j, \tag{13b}$$

the coefficients, $\tilde{v}^-_{jk}$, $\tilde{v}^+_{jk}$ and $\tilde{\mu}^-_j$, $\tilde{\mu}^+_j$, are given in Appendix A.1. Inserting (13) in Eq. (9), it results a 2D Helmholtz equation on the inner points, $i \in \{1,\ldots,N_x-1\}$, $j \in \{1,\ldots,N_z-1\}$

$$\sum_{k=1}^{N_x-1}\left\{(\mathscr{D}^2_x)_{ik} + (\mathscr{D}^2_x)_{i0}\tilde{v}^-_{jk} + (\mathscr{D}^2_x)_{iN_x}\tilde{v}^+_{jk}\right\}\tilde{u}_{kj} + \sum_{l=1}^{N_z-1}(\Lambda^2_z)_{jl}\tilde{u}_{il} - a\tilde{u}_{ij} = \tilde{f}_{ij} - (\mathscr{D}^2_x)_{i0}\tilde{\mu}^-_j - (\mathscr{D}^2_x)_{iN_x}\tilde{\mu}^+_j. \tag{14}$$

As a matter of fact, Eq. (14) can be seen as a set of (N_{z-1}) 1D modified Helmholtz equations, in the horizontal direction, if we consider that the Helmholtz constants are now equal to $a'_j = a - (\lambda_z)_j$.

Step 4: Diagonalisation.

In order to diagonalise the Helmholtz operator $\tilde{\mathscr{H}}$, i.e. the left part of Eq. (14), it is expressed as a sum of two operators: $\tilde{\mathscr{H}}_\tau$, the tensoriable part of the total operator and $\tilde{\mathscr{H}}_{cl}$, coming from the elimination of the mixed boundary conditions, which is not tensoriable. $\tilde{\mathscr{H}}_\tau$ can be written using tensor notation

$$\tilde{\mathscr{H}}_\tau = (\mathscr{D}^2_x)_{\text{int}} \otimes \mathbb{I}_z + \mathbb{I}_x \otimes (\Lambda^2_z) - a\mathbb{I}_x \otimes \mathbb{I}_z. \tag{15}$$

For $\tilde{\mathscr{H}}_{cl}$, the following notation is used:

$$(\tilde{\mathscr{H}}_{cl})_{ik}(j) = (\mathscr{D}^2_x)_{i0}\tilde{v}^-_{jk} + (\mathscr{D}^2_x)_{iN_x}\tilde{v}^+_{jk}. \tag{16}$$

The dependence of $\tilde{\mathscr{H}}_{cl}$ on j results in the loss of tensoriability of the Hemholtz operator. However, both $\tilde{\mathscr{H}}_\tau$ and $\tilde{\mathscr{H}}_{cl}$ are block diagonal as displayed in Appendix A.2. Thus $\tilde{\mathscr{H}}$ is block diagonal as a sum of two block diagonal matrices and each block can be independently diagonalised.

Step 5: To solve for u.

$\tilde{\mathscr{H}}(j)$ being the jth block of $\tilde{\mathscr{H}}$, the matrix of its eigenvectors, $\tilde{\mathscr{M}}_x(j)$, is such that

$$\tilde{\mathscr{M}}_x(j)^{-1}\tilde{\mathscr{H}}(j)\tilde{\mathscr{M}}_x(j) = \tilde{\Lambda}_x(j) \tag{17}$$

with $(\tilde{\Lambda}_x)_{ik}(j) = \delta_{ik}\tilde{\lambda}_{kj}$. The change of basis applied to $\tilde{u}$ and $\tilde{f}$ is performed as follows:

$$\tilde{\tilde{u}}_{ij} = \sum_{k=1}^{N_x-1}(\tilde{\mathscr{M}}_x(j)^{-1})_{ik}\tilde{u}_{kj} \quad \text{and} \quad \tilde{\tilde{f}}_{ij} = \sum_{k=1}^{N_x-1}(\tilde{\mathscr{M}}_x(j)^{-1})_{ik}\tilde{f}_{kj}.$$

The solution is then directly given by the relation: $\tilde{\tilde{u}}_{ij} = \tilde{\tilde{f}}_{ij}/(\tilde{\lambda}_{ij} - a)$.

It must be emphasised that the order of the steps is critical, and that independently diagonalising each block, in step 4, requires that the reduced second order operators are identical in the Helmholtz equation and the mixed boundary conditions.

This procedure is heavier on memory compared to Haldenwang et al.'s algorithm. Indeed, the change of basis here requires to store the $(N_x-1)^2$ elements of each $\mathscr{M}_z$ and $\mathscr{M}_z^{-1}$ matrices and the $(N_z-1)^2$ elements of the $\widetilde{\mathscr{M}}_x$ and $\widetilde{\mathscr{M}}_x^{-1}$ matrices, i.e. $2\times(N_x-1)^2\times(N_z-1)+2\times(N_z-1)^2$ elements instead of $2\times(N_x-1)^2+2\times(N_z-1)^2$ elements of 4 matrices. Nevertheless the number of operations performed for diagonalising the operator will be virtually the same as for successive diagonalisations, within a permutation of the solution field's indices. When compared to the inversion of the total operator, the proposed procedure is cheaper in memory and in computation time as it will be show in Section 4.3. Referring to step 4 of the algorithm, we shall now designate it as: *blocks diagonalisation*.

3.3. Extensions of the procedure

3.3.1. Neumann and Robin conditions

If the boundary conditions at $z=\pm1$ are $\partial u/\partial z=\gamma(x)$, the u values on the boundaries will be expressed as linear combinations of the inner values as follows:

$$u_{i0}=\sum_{l=1}^{N_z-1}\tilde{v}_l^-u_{il}+\gamma_i^-, \tag{18a}$$

$$u_{iN_z}=\sum_{l=1}^{N_z-1}\tilde{v}_l^+u_{il}+\gamma_i^+ \tag{18b}$$

and inserted in (7) and (8) (the coefficients $\tilde{v}_l^-$, $\tilde{v}_l^+$, γ_i^-, γ_i^+ are obtained as solutions of a linear system). The extension to Robin conditions is straightforward.

3.3.2. 3D configurations

The procedure can easily be adapted to 3D Cartesian configurations with mixed boundary conditions on one pair of parallel faces. Extension to 3D cylindrical configurations with mixed boundary conditions on the lateral surface and classical boundary conditions (Dirichlet, Neumann, Robin) on the extremities is briefly described in Appendix A.3. In that geometry, Gauss–Radau collocation points are used so as not to impose boundary condition on the central axis [2].

The 3D procedure can be resumed as follows:

Step 1: reduction of the discretised system by taking into account all the classical boundary conditions.
Step 2: changes of basis in order to diagonalise all the second derivative operators in the normal directions to these boundaries.
Step 3: reduction of the system by using the mixed boundary conditions.
Step 4: diagonalisation of the resulting Helmholtz operator $\tilde{\tilde{\mathscr{H}}}=\tilde{\tilde{\mathscr{H}}}_\tau+\tilde{\tilde{\mathscr{H}}}_{cl}$, where

$$\tilde{\tilde{\mathscr{H}}}_\tau=((\mathscr{D}_x^2))_{\text{int}}\otimes\mathbb{I}_y\otimes\mathbb{I}_z+\mathbb{I}_x\otimes\mathbb{I}_y\otimes(\Lambda_z^2)+\mathbb{I}_x\otimes(\Lambda_y^2)\otimes\mathbb{I}_z-a\mathbb{I}_x\otimes\mathbb{I}_y\otimes\mathbb{I}_z. \tag{19}$$

and

$$(\tilde{\tilde{\mathscr{H}}}_{cl})_{ik}(jl)=(\mathscr{D}_x^2)_{i0}\tilde{\tilde{v}}_{jkl}^-+(\mathscr{D}_x^2)_{iN_x}\tilde{\tilde{v}}_{jkl}^+. \tag{20}$$

Step 5: to solve for u.

The storage cost is equal to the 2D storage cost multiplied by the number of points in the third direction. The computation cost remains very likely to the cost of a successive diagonalisation procedure.

4. Validation

4.1. An analytical test case

The algorithm is now applied to the Helmholtz problem (1) and (2) where the source, f, and the coefficients, $\alpha_{1\pm}$, $\beta_{1\pm}$, $\gamma_{1\pm}(z)$, $\alpha_{2\pm}$, $\beta_{2\pm}$, $\gamma_{2\pm}(x)$, are given by

$$\begin{aligned} f &= -(2\pi^2 + a)(\sin(\pi x)\sin(\pi z) + \cos(\pi x)\cos(\pi z)) - a\ C, \\ \alpha_{1\pm} &= -\frac{1}{2}, \\ \beta_{1\pm} &= \pm 1, \\ \gamma_{1\pm}(z) &= -\frac{\pi^2}{2}\cos(\pi z) \mp \pi \sin(\pi z), \\ \alpha_{2\pm} &= 1, \\ \gamma_{2\pm}(x) &= -\cos(\pi x) + C. \end{aligned} \tag{21}$$

Of course, the chosen coefficients insure the compatibility of the boundary conditions in the corners of the domain. The analytical solution is the trigonometric function of x and z:

$$u = \sin(\pi x)\sin(\pi z) + \cos(\pi x)\cos(\pi z) + C. \tag{22}$$

This function does not cancel on the boundaries neither its normal derivatives to the boundaries. The constant C, related to the constant mode, is fixed to a non-zero value (here to 10) so as to avoid any cancellation of u, given rise to some problem in the calculation of the relative error defined as follows:

$$\varepsilon = \max_{x,z\in\Omega} \left| \frac{u_{\mathrm{cp}}(x,z) - u_{\mathrm{an}}(x,z)}{u_{\mathrm{an}}(x,z)} \right|,$$

where u_{cp} and u_{an}, respectively, are the computed and the analytical solutions.

Fig. 2 shows the evolution of the error as a function of the grid refinement, for two values of the Helmholtz constant a. The curves show very similar behaviours which can be extended to any positive value of a in particular to Poisson equation ($a = 0$). When refining the grid (from 5×5 to $\sim 20 \times 20$ nodes), the error rapidly and monotonically decreases down to 10^{-14} which corresponds to the convergence of the spectral accuracy with the number of modes. For finer grids, the error now increases (up to 10^{-11} for 250^2 points) due to the accumulation of round-off errors in the preprocessing calculation of the eigenvalues and eigenvectors as already mentioned by Haidvogel and Zang [4] and Haldenwang et al. [6].

4.2. An interface with surface viscosity

We now consider the problem of an opened channel of infinite extension containing two viscous incompressible fluids (I and II). The bottom of the channel is moving steadily in the longitudinal direction, carrying on the fluids which are separated by a plane interface with negligible mass. This configuration has been introduced by Prud'homme and Gatignol [13] to study the effect of an interface of two superposed immiscible fluids with constant shear surface viscosity (see Fig. 3). Assuming that the upper fluid is of negligible viscosity in comparison to the other and that the flow is lengthwise, laminar, and steady, the following equations for the velocity $\vec{V}_I = V_x\vec{e}_x + V_y\vec{e}_y + V_z\vec{e}_z$ can be written as

$$V_x = V_z = 0, \quad \frac{\partial^2 V_y}{\partial x^2} + \frac{\partial^2 V_y}{\partial z^2} = 0. \tag{23}$$

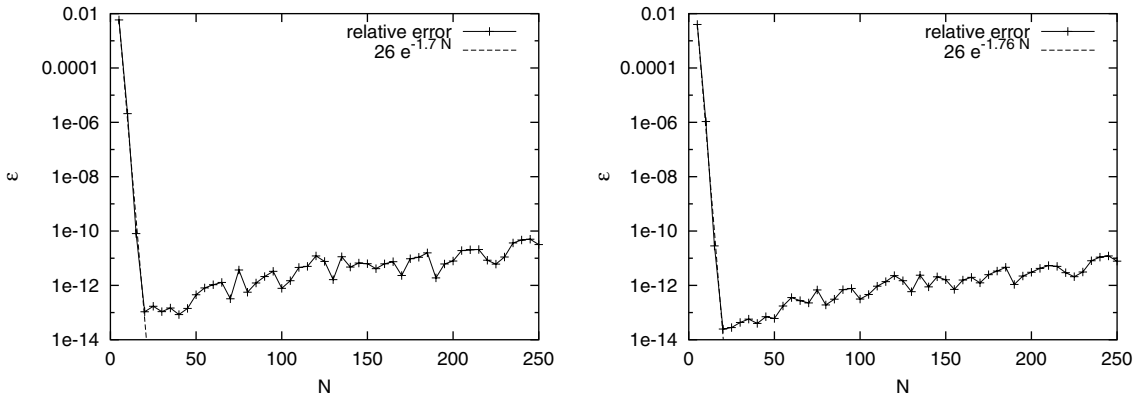

Fig. 2. Error of the computed solution versus the number N of collocation points in each direction, $N = N_x = N_z$ (square mesh), on a logarithmic scale.

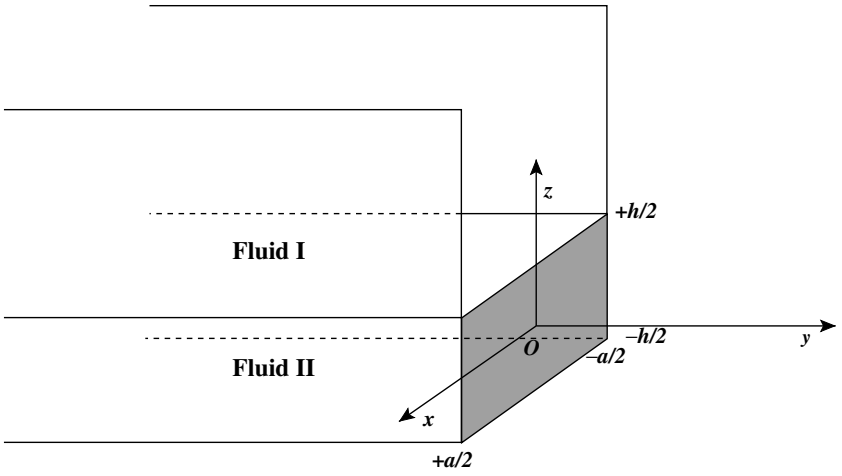

Fig. 3. Driven opened boat with interfacial viscosity.

Defining $A = h/a$, the aspect ratio, the boundary conditions are:

$$\text{on the vertical walls,} \qquad V_y = 0 \quad \text{at } x = \pm\frac{1}{2}, \tag{24a}$$

$$\text{on the free surface,} \qquad \frac{\partial V_y}{\partial z} = \hat{Vi}\frac{\partial^2 V_y}{\partial x^2} \quad \text{at } z = +\frac{A}{2}, \tag{24b}$$

$$\text{and on the bottom,} \qquad V_y = 1 \quad \text{at } z = -\frac{A}{2}, \tag{24c}$$

where $\hat{Vi} = \epsilon/(\mu_1 a)$, ϵ and μ_1 being the interface shear viscosity and fluid I viscosity, respectively. $\hat{Vi}$ and A have been fixed to 0.01 and 1. The solution can be analytically derived as a Fourier expansion:

$$V_y(x,z) = V_0 \sum_{m=1}^{\infty} \frac{4}{m\pi} \frac{\mathrm{Ch}(m\pi(z-\frac{A}{2})) - Vi\ m\pi\mathrm{Sh}(m\pi(z-\frac{A}{2}))}{\mathrm{Ch}(m\pi A) + Vi\ m\pi\mathrm{Sh}(m\pi A)} \mathrm{Sin}\left(m\pi\frac{x+1}{2}\right). \tag{25}$$

Due to the singularities of the boundary conditions at $(x,z) = (\pm 1/2, -A/2)$, the computation of (25) requires $\approx 5 \times 10^5$ modes to satisfy the top boundary condition with an error of 10^{-12} whereas $\approx 10^7$ modes are necessary to satisfy the bottom boundary condition with an error of 10^{-4}.

Fig. 4 displays the relative error, $E_{vsl} = |(V_{cfs}(N) - V_{cfs}(72))/V_{cfs}(72)|$, between the velocity at the center of the free surface, $V_{cfs}(N)$, calculated with N Chebyshev modes in each direction and the chosen reference value, $V_{cfs}(72)$, calculated with 72 modes in each direction. The error decreases as $\approx \mathrm{O}(N^2)^{-4}$. The deterioration of the convergence rate is clearly related to the corner singularities as already discussed by Haidvogel and Zang [4] for a similar problem.

4.3. A thermal configuration

The aim of this section is twice: to estimate the CPU cost of our algorithm and to compare its results with those of the literature on a stability thresholds determination which requires high precision.

A large amount of work has been done on the classical Bénard problem in a closed cavity. Most of which concerns a volume of fluid bounded above and below by isothermal surfaces and laterally by adiabatic surfaces. In a few papers, the effect of conducting lateral boundaries on the stability of the fluid is studied [5].

The physical case here considered consists of a 2D rectangular cavity filled with an incompressible Boussinesq viscous fluid of thermal diffusivity κ_f and kinematic viscosity v (see Fig. 5). The perfectly conducting top and bottom surfaces are isothermal with a temperature difference equal to

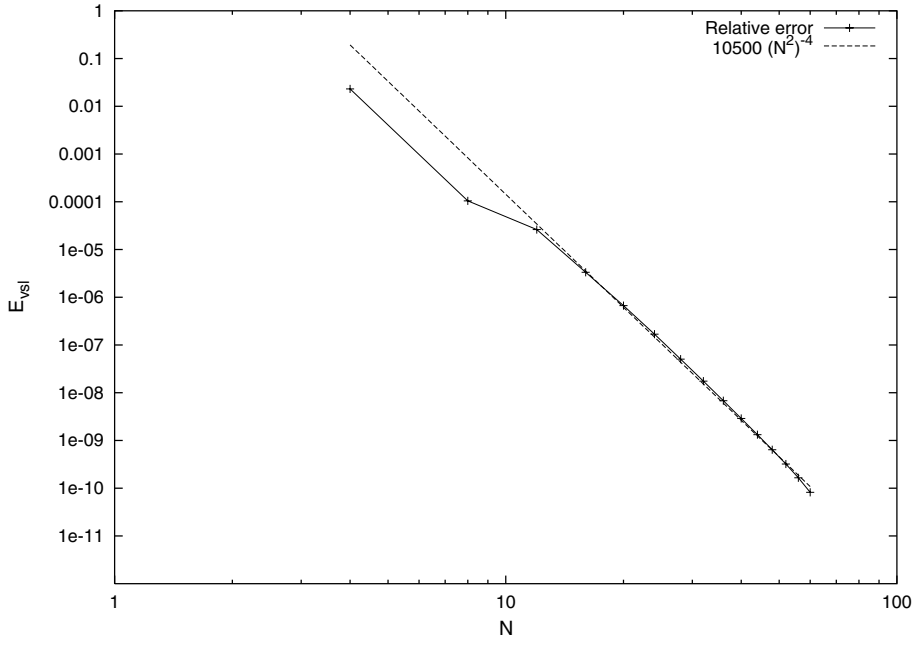

Fig. 4. Evolution of the relative error for $N \in [1, 60]$, the results at $N = 72$ being chosen as reference values.

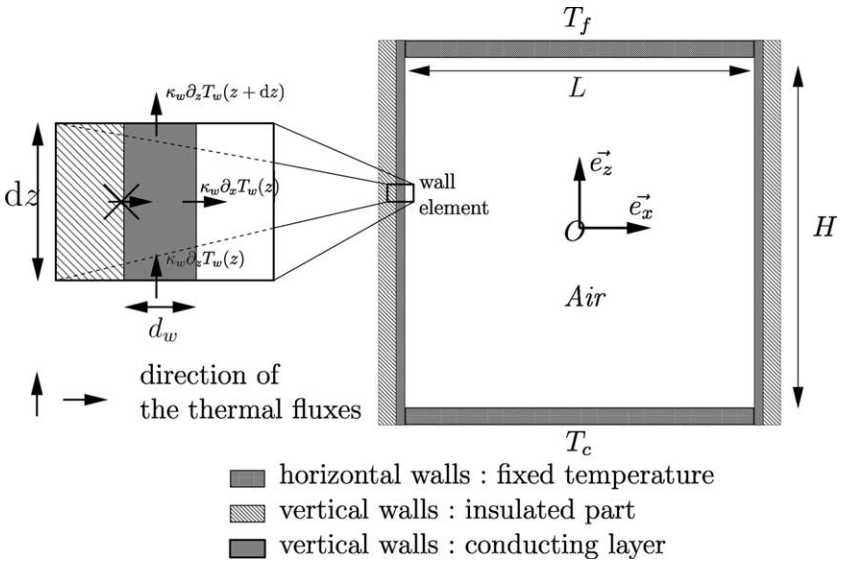

Fig. 5. The thermal configuration.

$\Delta T = T_{\text{bottom}} - T_{\text{top}} > 0$. The lateral walls are composed of a thin layer of conducting material which is isolated outside.

The problem is made non-dimensional by choosing the characteristic length, time, temperature and pressure scales, respectively, equal to the height of the cavity H, the thermal time $t_{\text{ref}} = H^2/\kappa_{\text{f}}$, $\theta = (T - T_{\text{r}})/\Delta T$ with T_{r} the mean temperature, and $p_{\text{ref}} = \rho_0 \kappa_{\text{f}}^2 H^{-2}$, with ρ_0 the fluid density at temperature T_{r}. Defining the aspect ratio $A = L/H$, the Prandtl number $Pr = \nu/\kappa_{\text{f}}$, and the Rayleigh number $Ra = g\beta\Delta T H^3/(\nu\kappa_{\text{f}})$, with g the gravitational acceleration and β the thermal expansion coefficient at temperature T_{r}, the Navier–Stokes and energy equations under Boussinesq approximation are:

$$\frac{\partial u}{\partial t} + u\frac{\partial u}{\partial x} + w\frac{\partial u}{\partial z} = -\frac{\partial p}{\partial x} + Pr\left(\frac{\partial^2}{\partial x^2} + \frac{\partial^2}{\partial z^2}\right)u, \tag{26a}$$

$$\frac{\partial w}{\partial t} + u\frac{\partial w}{\partial x} + w\frac{\partial w}{\partial z} = -\frac{\partial p}{\partial z} + Pr\left(\frac{\partial^2}{\partial x^2} + \frac{\partial^2}{\partial z^2}\right)w + Ra \cdot Pr \cdot \theta, \tag{26b}$$

$$\frac{\partial \theta}{\partial t} + u\frac{\partial \theta}{\partial x} + w\frac{\partial \theta}{\partial z} = \left(\frac{\partial^2}{\partial x^2} + \frac{\partial^2}{\partial z^2}\right)\theta, \tag{26c}$$

$$\frac{\partial u}{\partial x} + \frac{\partial v}{\partial z} = 0. \tag{26d}$$

These conservation equations are completed with the boundary conditions:

$$u = w = 0 \quad \text{on all the surfaces,} \tag{27a}$$

$$\theta(x, -A/2) = 1/2, \quad \theta(x, A/2) = -1/2, \tag{27b}$$

and, as proposed by Buell and Catton [5], to take into account the heat conduction in the lateral wall, the following condition, mixing normal and tangential derivatives, is introduced:

$$\frac{\partial \theta}{\partial x} = \pm C_{\text{w}} \frac{\partial^2 \theta}{\partial z^2} \quad \text{at } x = \pm A/2, \tag{27c}$$

where $C_w = (\kappa_w d_w)/(\kappa_f H)$ is the wall admittance with κ_w the wall conductivity and d_w the wall thickness with $d_w/H \ll 1$. If $C_w = 0$, the wall is adiabatic; if $C_w \to \infty$, it is perfectly conducting. A and Pr are, respectively, fixed to 1 and 0.71 in this study.

The expansion of the velocity and temperature fields in Chebyshev series leads to a system of ordinary temporal differential equations which is solved by using a second order finite difference time-stepping scheme with an implicit treatment of the diffusion terms, the others being explicitly evaluated. A projection–diffusion algorithm, described at length in [9,12], is used to uncouple the velocity and pressure fields.

4.3.1. Computational time costs comparison

As a measure of the efficiency of our algorithm, we computed 2000 time steps in a Rayleigh–Bénard configuration with lateral adiabatic walls ($C_w = 0$), for a variety of mesh refinements, and compared the elapsed times with those obtained by successive diagonalisations and direct inversion. The results of these simulations are presented in Table 1, in seconds. For each algorithm, the first column yields the initialisation time (calculation of the operators, diagonalisation, inversion, etc.), the second yields the elapsed time after 2000 iterations of the temporal scheme solving Navier–Stokes and energy equations.

It appears that the initialisation and time iterations parts both are very costly in the direct inversion method. The blocks diagonalisation algorithm exhibits a behaviour in agreement with our expectations: the initialisation step is over ten times slower than for successive diagonalisations but is very efficient compared to direct inversion. The temporal part costs are of the same order in the diagonalisation procedures, the differences can be attributed to the implementation because the code using successive diagonalisations has been optimised whereas our code is still perfectible. It must be emphasised that direct inversion is limited to small numbers of grid points whereas blocks diagonalisation allows to work with reasonable meshes (of course the maximum number of grid points depends on the available memory of the computer).

4.3.2. Convection thresholds as a benchmark problem

The symmetries of our configuration ($A = 1$) are such that the transition between the conductive and the convective flows in Rayleigh–Bénard configuration corresponds to a super-critical pitchfork bifurcation of the steady state at a critical Rayleigh value, Ra_c. The linear stability theory predicts a linear evolution of infinitesimal perturbations of the steady state near the bifurcation threshold. The growth rates of the velocity components and the temperature, due to small initial perturbations of the steady state have been calculated at three points of the cavity for Ra values near Ra_c. The global growth rates have been taken as the mean value of each set of these 9 values. The critical Rayleigh value has then been obtained through a linear regression calculated on, at least, 5 mean values of growth rates of the order 10^{-2}. Fig. 6 gives Ra_c as a function of the wall coefficient C_w. At $C_w = 0$, $Ra_c = 2584.99$ which agrees with the value $Ra_c = 2585.03$ obtained by Platten and Legros [7]. The threshold value increases with C_w on the interval $C_w \in (0.08, 9)$. The value $Ra_c = 5010.30$, calculated for $C_w = 10^{-3}$, can be compared to the value $Ra_c = 5035$ obtained by Davis [1] for perfectly conducting walls but on a 3D configuration; it is the only value found in the literature.

Table 1
Computation times in second, for a Rayleigh–Bénard problem with adiabatic lateral walls, at $Ra = 3500$, $Pr = 0.71$, $dt = 1 \times 10^{-3}$

Mesh size	Tensoriable problem successive diagonalisations		Blocks diagonalisation		Helmholtz operator direct inversion	
15×15	0,007	60,233	0,151	65,958	2,607	80,500
30×30	0,395	409,875	1,516	451,951	185,572	761,260
50×50	1,618	1790,656	9,619	1990,806	6804,348	4488,353
100×100	11,803	13748,125	128,036	15396,710	–	–
150×150	39,020	45823,149	612,230	51242,103	–	–

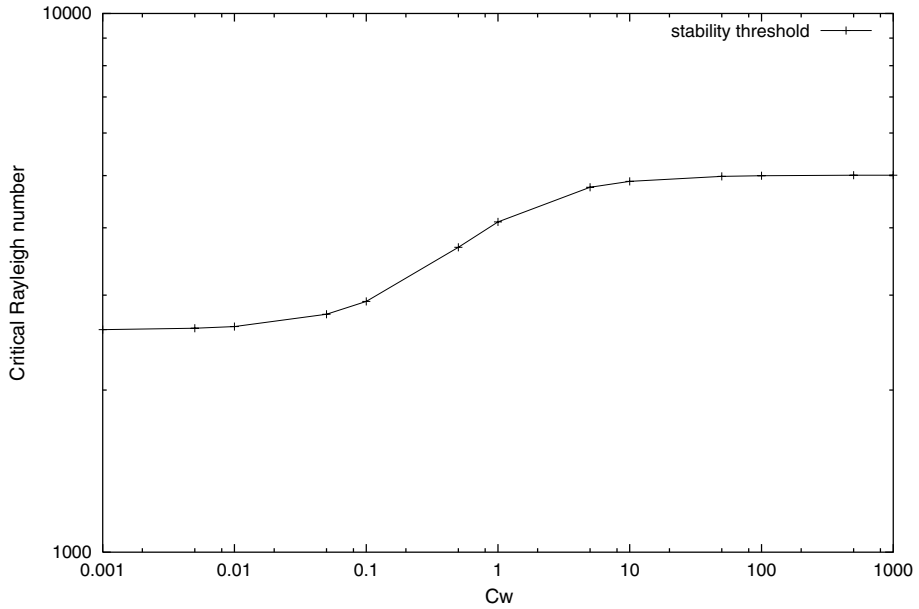

Fig. 6. The critical Rayleigh number, Ra_c, as a function of the non-dimensional wall coefficient C_w (in log/log scales).

5. Conclusion

We have extended the successive diagonalisation technique solving the Helmholtz problem with homogeneous Robin boundary conditions to the case of boundary conditions mixing a second order tangential derivative with a first order normal derivative. The algorithm does not increase the computation time but requires more memory storage. The spectral accuracy is preserved. The application of the procedure to the determination of the transition thresholds between the conductive and convective regimes of an incompressible fluid in a rectangular cavity heated from below, with partially conducting vertical walls, has shown the dependence of the critical Rayleigh number on the wall conductivity.

Acknowledgements

The authors thank the CRI (Centre de Ressources Informatiques de l'Université d'Orsay) for the use of its computing facilities and the support they received.

Appendix A

A.1. Appendix 1

To solve the linear system (A.1):

$$(\tilde{\alpha}_{1-}(j) + \tilde{\beta}_{1-}(\mathscr{D}_x)_{00})\tilde{u}_{0j} + \tilde{\beta}_{1-}\sum_{k=1}^{N_x-1}(\mathscr{D}_x)_{0k}\tilde{u}_{kj} + \tilde{\beta}_{1-}(\mathscr{D}_x)_{0N_x}\tilde{u}_{N_xj} = \tilde{\gamma}'_{1-}(j), \tag{A.1a}$$

$$(\tilde{\alpha}_{1+}(j)+\tilde{\beta}_{1+}(\mathscr{D}_x)_{N_xN_x})\tilde{u}_{N_xj}+\tilde{\beta}_{1+}\sum_{k=1}^{N_x-1}(\mathscr{D}_x)_{N_xk}\tilde{u}_{kj}+\tilde{\beta}_{1+}(\mathscr{D}_x)_{N_x0}\tilde{u}_{0j}=\tilde{\gamma}'_{1+}(j) \tag{A.1b}$$

in $\tilde{u}_{0j}$, $\tilde{u}_{N_xj}$ is straightforward.

Through the following combinations of the two set of equations:

$$\begin{cases}(\tilde{\alpha}_{1+}(j)+\tilde{\beta}_{1+}(\mathscr{D}_x)_{N_xN_x})\times\text{(A.1a)}-\tilde{\beta}_{1-}(\mathscr{D}_x)_{0N_x}\times\text{(A.1b)},\\ \tilde{\beta}_{1+}(\mathscr{D}_x)_{N_x0}\times\text{(A.1a)}-(\tilde{\alpha}_{1-}(j)+\tilde{\beta}_{1-}(\mathscr{D}_x)_{00})\times\text{(A.1b)}\end{cases}$$

we obtain:

$$\begin{aligned}&\sum_{k=1}^{N_x-1}\{(\tilde{\alpha}_{1+}(j)+\tilde{\beta}_{1+}(\mathscr{D}_x)_{N_xN_x})(\tilde{\beta}_{1-}(\mathscr{D}_x)_{0k})-(\tilde{\beta}_{1-}(\mathscr{D}_x)_{0N_x})(\tilde{\beta}_{1+}(\mathscr{D}_x)_{N_xk})\}\tilde{u}_{kj}\\ &\quad+\{(\tilde{\alpha}_{1+}(j)+\tilde{\beta}_{1+}(\mathscr{D}_x)_{N_xN_x})(\tilde{\alpha}_{1-}(j)+\tilde{\beta}_{1-}(\mathscr{D}_x)_{00})-(\tilde{\beta}_{1-}(\mathscr{D}_x)_{0N_x})(\tilde{\beta}_{1+}(\mathscr{D}_x)_{N_x0})\}\tilde{u}_{0j}\\ &\qquad=(\tilde{\alpha}_{1+}(j)+\tilde{\beta}_{1+}(\mathscr{D}_x)_{N_xN_x})\tilde{\gamma}'_{1-}(j)-(\tilde{\beta}_{1-}(\mathscr{D}_x)_{0N_x})\tilde{\gamma}'_{1+}(j),\\ &\sum_{k=1}^{N_x-1}\{(\tilde{\beta}_{1+}(\mathscr{D}_x)_{N_x0})(\tilde{\beta}_{1-}(\mathscr{D}_x)_{0k})-(\tilde{\alpha}_{1-}(j)+\tilde{\beta}_{1-}(\mathscr{D}_x)_{00})(\tilde{\beta}_{1+}(\mathscr{D}_x)_{N_xk})\}\tilde{u}_{kj}\\ &\quad+\{(\tilde{\beta}_{1+}(\mathscr{D}_x)_{N_x0})(\tilde{\beta}_{1-}(\mathscr{D}_x)_{0N_x})-(\tilde{\alpha}_{1-}(j)+\tilde{\beta}_{1-}(\mathscr{D}_x)_{00})(\tilde{\alpha}_{1+}(j)+\tilde{\beta}_{1+}(\mathscr{D}_x)_{N_xN_x})\}\tilde{u}_{N_xj}\\ &\qquad=(\tilde{\beta}_{1+}(\mathscr{D}_x)_{N_x0})\tilde{\gamma}'_{1-}(j)-(\tilde{\alpha}_{1-}(j)+\tilde{\beta}_{1-}(\mathscr{D}_x)_{00})\tilde{\gamma}'_{1+}(j).\end{aligned} \tag{A.2}$$

We define $\tilde{v}^-_{jk}$, $\tilde{v}^+_{jk}$ and $\tilde{\mu}^-_j$, $\tilde{\mu}^+_j$ as

$$\tilde{v}^-_{jk}=\frac{(\tilde{\beta}_{1-}(\mathscr{D}_x)_{0N_x})(\tilde{\beta}_{1+}(\mathscr{D}_x)_{N_xk})-(\tilde{\alpha}_{1+}(j)+\tilde{\beta}_{1+}(\mathscr{D}_x)_{N_xN_x})(\tilde{\beta}_{1-}(\mathscr{D}_x)_{0k})}{(\tilde{\alpha}_{1+}(j)+\tilde{\beta}_{1+}(\mathscr{D}_x)_{N_xN_x})(\tilde{\alpha}_{1-}(j)+\tilde{\beta}_{1-}(\mathscr{D}_x)_{00})-(\tilde{\beta}_{1-}(\mathscr{D}_x)_{0N_x})+(\tilde{\beta}_{1+}(\mathscr{D}_x)_{N_x0})},$$

$$\tilde{v}^+_{jk}=\frac{(\tilde{\beta}_{1+}(\mathscr{D}_x)_{N_x0})(\tilde{\beta}_{1-}(\mathscr{D}_x)_{0k})-(\tilde{\alpha}_{1-}(j)+\tilde{\beta}_{1-}(\mathscr{D}_x)_{00})(\tilde{\beta}_{1+}(\mathscr{D}_x)_{N_xk})}{(\tilde{\alpha}_{1-}(j)+\tilde{\beta}_{1-}(\mathscr{D}_x)_{00})(\tilde{\alpha}_{1+}(j)+\tilde{\beta}_{1+}(\mathscr{D}_x)_{N_xN_x})-(\tilde{\beta}_{1+}(\mathscr{D}_x)_{N_x0})+(\tilde{\beta}_{1-}(\mathscr{D}_x)_{0N_x})},$$

$$\tilde{\mu}^-_j=\frac{(\tilde{\alpha}_{1+}(j)+\tilde{\beta}_{1+}(\mathscr{D}_x)_{N_xN_x})\tilde{\gamma}'_{1-}(j)-(\tilde{\beta}_{1-}(\mathscr{D}_x)_{0N_x})\tilde{\gamma}'_{1+}(j)}{(\tilde{\alpha}_{1+}(j)+\tilde{\beta}_{1+}(\mathscr{D}_x)_{N_xN_x})(\tilde{\alpha}_{1-}(j)+\tilde{\beta}_{1-}(\mathscr{D}_x)_{00})-(\tilde{\beta}_{1-}(\mathscr{D}_x)_{0N_x})(\tilde{\beta}_{1+}(\mathscr{D}_x)_{N_x0})},$$

$$\tilde{\mu}^+_j=\frac{(\tilde{\alpha}_{1-}(j)+\tilde{\beta}_{1-}(\mathscr{D}_x)_{00})\tilde{\gamma}'_{1+}(j)-(\tilde{\beta}_{1+}(\mathscr{D}_x)_{N_x0})\tilde{\gamma}'_{1-}(j)}{(\tilde{\alpha}_{1-}(j)+\tilde{\beta}_{1-}(\mathscr{D}_z)_{00})(\tilde{\alpha}_{1+}(j)+\tilde{\beta}_{1+}(\mathscr{D}_x)_{N_xN_x})-(\tilde{\beta}_{1+}(\mathscr{D}_x)_{N_x0})(\tilde{\beta}_{1-}(\mathscr{D}_x)_{0N_x})},$$

which simplifies the expression of $\tilde{u}_{0j}$ and $\tilde{u}_{N_xj}$:

$$\tilde{u}_{0j}=\sum_{k=1}^{N_x-1}\tilde{v}^-_{jk}\tilde{u}_{kj}+\tilde{\mu}^-_j, \tag{A.3a}$$

$$\tilde{u}_{N_xj}=\sum_{k=1}^{N_x-1}\tilde{v}^+_{jk}\tilde{u}_{kj}+\tilde{\mu}^+_j. \tag{A.3b}$$

A.2. Appendix 2

The structures of the block diagonal matrices $\tilde{\mathscr{H}}_\tau$ and $\tilde{\mathscr{H}}_{cl}$ are:

$$\tilde{\mathcal{H}}_\tau = \begin{pmatrix} \left((\mathcal{D}_x^2)_{int} + (\lambda_z)_1 \mathbb{I}_x - a\,\mathbb{I}_x\right) & 0 & \cdots & 0 \\ 0 & \left((\mathcal{D}_x^2)_{int} + (\lambda_z)_2 \mathbb{I}_x - a\,\mathbb{I}_x\right) & \ddots & \vdots \\ \vdots & \ddots & \ddots & 0 \\ 0 & \cdots & 0 & \left((\mathcal{D}_x^2)_{int} + (\lambda_z)_{N_z-1} \mathbb{I}_x - a\,\mathbb{I}_x\right) \end{pmatrix}, \tag{A.4}$$

and

$$\tilde{\mathcal{H}}_{cl} = \begin{pmatrix} \tilde{\mathcal{H}}_{cl}(1) & 0 & \cdots & 0 \\ 0 & \tilde{\mathcal{H}}_{cl}(2) & \ddots & \vdots \\ \vdots & \ddots & \ddots & 0 \\ 0 & \cdots & 0 & \tilde{\mathcal{H}}_{cl}(N_z - 1) \end{pmatrix}. \tag{A.5}$$

A.3. Appendix 3

Let us consider the case of a 3D Helmholtz problem in cylindrical coordinates, (r,φ,z), defined on the domain $\Omega \equiv]0,1]\times[0,2\pi[\times[-\frac{1}{2},+\frac{1}{2}]$

$$\frac{1}{r}\frac{\partial}{\partial r}\left(r\frac{\partial u}{\partial r}\right)+\frac{1}{r^2}\frac{\partial^2 u}{\partial \varphi^2}+\frac{\partial^2 u}{\partial z^2}-au=f. \tag{A.6}$$

The mixed derivatives condition can be applied on the lateral side of the cylinder together with Dirichlet conditions on the remaining sides

$$\begin{aligned}&\alpha_1\left(\frac{1}{r^2}\frac{\partial^2 u}{\partial \varphi^2}+\frac{\partial^2 u}{\partial z^2}\right)+\beta_1\frac{\partial u}{\partial r}=\gamma_1(\varphi,z) \quad \text{at } r=1,\\ &\alpha_{2\pm}u=\gamma_{2\pm}(r,\varphi) \quad \text{at } z=\pm 1.\end{aligned} \tag{A.7}$$

Real functions, $f(r,\varphi,z)$, periodic in φ, are approximated by their truncated discrete Fourier series as

$$f(r_i,\varphi_k,z_j)=\Re\left(\frac{1}{N_\varphi}\sum_{0\leqslant n<N_\varphi}\tilde{f}_k(r_i,z_j)\mathrm{e}^{in\varphi_k}\right).$$

The field u is expanded using Chebyshev polynomial series with classical Gauss–Radau and Gauss–Lobatto collocation points in the radial and axial directions, respectively. The collocation points in $\hat{e}_\varphi$ are imposed by the use of the discrete Fourier transform

$$2r_i-1=+\cos\left(\frac{2(N_r-i)\pi}{2N_r+1}\right), \quad i\in\{0,\ldots,N_r\}, \tag{A.8a}$$

$$z_j=-\cos\left(\frac{j\pi}{N_z}\right), \quad j\in\{0,\ldots,N_z\}, \tag{A.8b}$$

$$\varphi_k=\frac{2\pi k}{N_\varphi}, \quad k\in\{0,\ldots,N_\varphi-1\}. \tag{A.8c}$$

Using the following discrete notation $\tilde{f}_{(k)ij}=\tilde{f}_k(ij)$, (A.6), (A.7), respectively, become

$$\left[\frac{1}{r}\frac{\partial}{\partial r}\left(r\frac{\partial}{\partial r}\right)-\frac{k^2}{r^2}\right]\tilde{u}_{(k)ij}+\frac{\partial^2\tilde{u}_{(k)ij}}{\partial z^2}-a\tilde{u}_{(k)ij}=\tilde{f}_{(k)ij} \quad \text{for } k=\{0,\ldots,N_\varphi-1\}, \tag{A.9}$$

and

$$0\leqslant k<N_\varphi\begin{cases}\tilde{\alpha}_1\left(-\frac{k^2}{r^2}\tilde{u}_{(k)N_rj}+\frac{\partial^2\tilde{u}_{(k)N_rj}}{\partial z^2}\right)+\tilde{\beta}_1\frac{\partial\tilde{u}_{(k)N_rj}}{\partial r}=\tilde{\gamma}_{1(k)}(j) & \text{at } r=1,\\ \tilde{\alpha}_{2\pm}\tilde{u}_{(k)i|_0^{N_z}}=\tilde{\gamma}_{2\pm(k)}(i) & \text{at } z=\pm 1.\end{cases} \tag{A.10}$$

Eqs. (A.9) and (A.10) can be reorganised as a set of N_φ equations in (r,z) plus the corresponding boundary conditions. The procedure described in Section 3.2 can then be applied. Owing to the Gauss–Radau grid, step 3 is simplified, Eqs. (11) and (12), being replaced by

$$\left(\tilde{\tilde{\alpha}}_{1(k)}(j)+\tilde{\tilde{\beta}}_1(\mathscr{D}_r)_{N_rN_r}\right)\tilde{\tilde{u}}_{(k)N_rj}+\tilde{\tilde{\beta}}_1\sum_{m=0}^{N_r-1}(\mathscr{D}_r)_{N_rm}\tilde{\tilde{u}}_{(k)mj}=\tilde{\tilde{\gamma}}'_{1(k)}(j) \tag{A.11}$$

with $\tilde{\tilde{\alpha}}_{1(k)}(j)=(\lambda_{z(k)}(j)-\frac{k^2}{r^2})\tilde{\alpha}_{1(k)}(j)$. The expression of $\tilde{\tilde{u}}_{(k)N_rj}$ as a function of the inner points is straightforward.

References

[1] S.H. Davis, Convection in a box, J. Fluid Mech. 30 (1967) 465–478.
[2] C. Canuto, M.Y. Hussaini, A. Quarteroni, T. Zang, Spectral Methods in Fluids Dynamics, Springer, Berlin, 1977.
[3] D. Gottlieb, S.A. Orszag, Numerical Analysis of Spectral Methods: Theory and Applications, SIAM, Philadelphia, 1977.
[4] D.B. Haidvogel, T. Zang, The accurate solution of Poisson's equation by expansion in Chebyshev polynomials, J. Comput. Phys. 30 (1979) 167–180.
[5] J.C. Buell, I. Catton, The effect of wall conduction on the stability of a fluid in a right circular cylinder heated from below, J. Heat Transfer 105 (1983) 255–260.
[6] P. Haldenwang, G. Labrosse, S. Abboudi, M. Deville, Chebyshev 3-D spectral and 2-D pseudospectral solvers for the Helmholtz equation, J. Comput. Phys. 55 (1984) 115–128.
[7] J.K. Platten, J.C. Legros, Convection in Liquids, Springer, Berlin, 1984.
[8] H. Dang-Vu, C. Delcarte, An accurate solution of the Poisson equation by the Chebyshev collocation method, J. Comput. Phys. 104 (1993) 211–220.
[9] A. Batoul, H. Khallouf, G. Labrosse, Une méthode de résolution directe (pseudospectrale) du problème de Stokes 2D/3D instationnaire. Application à la cavité entrainée carrée, C. R. Acad. Sci. Ser. II 319 (1994) 1455.
[10] V.C. Regnier, P.M. Parmentier, G. Lebon, J.K. Platten, Numerical simulations of interface viscosity effects on thermoconvective motion in two-dimensional rectangular boxes, Int. J. Heat Mass Transfer 14 (1995) 2539–2548.
[11] C. Delcarte, G. Labrosse, S. Nguyen, Non-homogeneous boundary conditions in collocation spectral method, in: Proceedings of the ECCOMAS CFD Cnference, Swansea, UK, September 4–7, 2001.
[12] E. Leriche, G. Labrosse, High-order direct Stokes solvers with or without temporal splitting: numerical investigations of their comparative properties, SIAM J. Sci. Comput. 22 (N4) (2001) 1386–1410.
[13] R. Gatignol, R. Prud'homme, Mechanical and Thermomecanical Modelling of Fluid Interfaces, Series on Advances in Mathematics for Applied Sciences, vol. 58, World Scientific, Singapore, 2001.